Turbulent flame propagation with pressure oscillation in the end gas region of confined combustion chamber equipped with different perforated plates

Lei Zhou[a], Dongzhi Gao[a], Jianfu Zhao[a], Haiqiao Wei[a,*], Xiaojun Zhang[a], Zailong Xu[a], Rui Chen[a,b]

[a] State Key Laboratory of Engines, Tianjin University, Tianjin, 300072, China

[b] Department of Aeronautical and Automotive Engineering, Loughborough University, LE11 3TU, United Kingdom

(Accepted by Combustion and Flame, January 2018)

*Corresponding author: Haiqiao Wei
Address: 92 Weijin Road, Nankai District, Tianjin, P. R. China
Tel.: +86-22-27402609
Email: whq@tju.edu.cn

Abstract

Experiments were conducted in a newly designed constant volume combustion chamber with a perforated plate by varying the initial conditions. Hydrogen-air mixtures were used and the turbulent flame, shock wave, and the processes of flame-shock interactions were tracked via high-speed Schlieren photography. The effects of hole size and porosities on flame and shock wave propagation, intensity of the shock wave and pressure oscillation in closed combustion chamber were analyzed in detail. The effect of interactions between the turbulent flame and reflected shock or acoustic wave on the turbulent flame propagation was comprehensively studied during the present experiment. The results demonstrated that flame front propagation velocity and pressure oscillation strongly depend on the hole size and porosities of the perforated plate. The flame front propagation velocity in the end gas region increases as hole size increases and porosity decreases. The flame front propagation intensity in the end region of a confined space is strongly relevant to two competing effects: the initial turbulent formation and turbulent flame development. The experimental results indicated that an oscillating flame is associated with both the reflected shock wave and the acoustic wave. Meanwhile, different turbulent flame propagations and combustion modes were observed.

Keywords: flame acceleration; shock wave; flame-shock interaction; pressure oscillation; oscillating combustion

1. Introduction

The turbulent flame is one of the most interesting parts of combustion science and industry systems. Due to its huge complexity and nonlinear combustion features, progress in understanding and predicting a turbulent flame is still extremely challenging at present [1-5]. Particularly, in a closed space, such as an internal combustion engine and fire safety area, turbulent flame propagation with induced pressure oscillation is strongly related to energy efficiency, safety, emissions, etc. The understanding of turbulent flame propagation in a confined space is still a vital obstacle for quantitatively understanding and predicting the combustion phenomenon, including the knocking combustion in gasoline engines, the interaction between the flame and shock/acoustic wave, and the deflagration to detonation transition (DDT) [4]. It is well known that flame propagation in a duct filled with obstacles can accelerate to a fast flame [4, 6, 7]. Therefore, based on previous studies, a newly designed experimental apparatus is used to investigate the turbulent flame propagation process with high-amplitude pressure oscillation in a small confined chamber with perforated plate.

Significant advances have been made over the past years in the understanding of flame propagation at the presence of obstacles [8, 9]. A great deal of effort [6-13] has been spent on studying the turbulent flame acceleration mechanism in channels equipped obstacles in recent decades. Bychkov et al.[4] noted that the flame acceleration in long tubes equipped with obstacles is induced by delayed burning between the obstacles. It can generate a powerful jet flow driving an extremely fast flame velocity [4, 14]. In addition, the well-known Kelvin–Helmholtz (K–H) and Rayleigh–Taylor (R–T) instabilities also have significant contribution to the flame acceleration when the flame is suddenly accelerated over an obstacle or through a vent. Previous studies have significantly improved our understanding of the flame acceleration process. However, turbulent combustion still remains one of the most intensively studied but least understood phenomena in combustion theory [8, 9]. In turbulent flame propagation, it involves two mechanisms of turbulent flames, the turbulent flame self-acceleration mechanism [5, 15, 16] and interactions between a turbulent flame and shock wave or compression wave (acoustic wave) [7, 14, 17-20]. A common conclusion is that the self-acceleration of a turbulent flame is related to the intensity of hydrodynamic instability as well as that of diffusional-thermal instability with the increase of flame surface. The interactions of reflected shocks with a flame or turbulent flame have been widely used to investigate flame instabilities transition to turbulence, and most recently, the deflagration to detonation transition (DDT) [21]. Furthermore, the transient flame-vortex interaction is the key process in the

description of an accelerating flame propagation through obstacles. The resulting flame-vortex interaction intensifies the rate of flame propagation and pressure rise. For instance, Di Sarli et al. [22-27] well and comprehensively investigated the unsteady coupling of the propagating flame and the flow field at the wake of obstacles by means of both particle image velocimetry (PIV) and large eddy simulation (LES). They clearly demonstrated a satisfactory agreement in terms of shape of the accelerating flame propagation, flame arrival times, spatial profile of the flame speed, pressure time history, and velocity vector fields. The flame- vortex or flow interaction finally improved the flame acceleration.

Based on the above theory fundamentals including the flame acceleration and flame-shock interactions, a number of experimental studies [12, 13, 28-30] have demonstrated the influence of obstacle spacing or scale on the flame propagation process. The work by Ciccarelli et al. [31] demonstrated that the detonation initiation due to shock reflection is roughly the same for the different blockage ratio (BR) reflector perforated plates tested. But, the work was carried out in a long detonation tube. Another work [30] was performed to study the effect of obstacle size and spacing on the initial stage of flame acceleration in a rough tube. The results presented that for the lower blockage ratio plates, the plate size did not have much effect on the flame acceleration. However, for a higher BR, the plate size had a strong effect on the run up distance corresponding to the spacing of the perforated plates. A serial of further works were conducted by Ciccarelli et al. [32, 33].

In other work by Abdulmajid [28], the effects of obstacle scale with the same BR on the flame speed and overpressure were investigated. The obstacle with two flat bars obtained maximum overpressure compared with that with four flat bars. Moreover, several studies regarding the mechanism of detonation attenuation by a porous medium were carried out. A novel mechanism was identified, where each shock reflection from a porous medium gives rise to significant enhancement of the gas reactivity. Recently, similar studies were performed. A flame passing through multiple cylindrical obstacles could generate high speed deflagrations at different obstacle configurations and blockage ratios.

Hall et al. [34] studied the effects of the number and location of solid obstacles on the rate of propagation of turbulent premixed flames. It is found that while the peak overpressure increases with increasing number of grids or baffle plates. After this work, Masri et al.[35] performed a comparative

study of turbulent premixed flames propagating past repeated obstacles. They found that for all fuels the peak pressure as well as the rate change of pressure increases with increasing blockage ratio (BR) and with decreasing separation between successive baffles. But, there works more focus on the pressure evolution. Maeda et al. [36] investigated the deflagration-to-detonation transition in a channel with different heights of obstacles. It is found that the initial flame acceleration showed almost the same pattern for different heights of obstacles. But, in the downstream region the flame front velocity for highest height reaches the sound speed. Furthermore, Valiev et al. [37] provided details of the theory and numerical modeling of the flame acceleration for various blockage ratios and various spacing between the obstacles in a channel with one open end and one close end. Gamezo et al.[38] demonstrated the competing effects of high blockage ratio: larger obstacles promote non-uniform flow and they also weaken shocks diffracting over large obstacles. Consequently, the DDT occurrence is affected. Similarly, Goodwin et al. [39] adopted the numerical simulations to investigate the effect of decreasing blockage ratio on DDT in an infinitely long rectangular channel. They pointed out different blockage ratios have different mechanisms and in a certain range the DDT can occur.

Although significant effort has been devoted to the flame acceleration and detonations combustion of a flame propagating through repeated obstacles or porous media, previous experimental studies did not completely address the turbulent flame propagation mechanism with high pressure oscillation in a confined space, especially a controlled turbulent flame. This problem is, of course, of prime importance to the design of engines, such as knock suppression in spark ignition engine. Furthermore, the interaction between a flame and shock wave is always accompanied by acoustic oscillations, which can lead to significant overpressures and pressure oscillations within a confined space [11, 40]. However, the amplitude of pressure oscillations or overpressures is very small. For a strong pressure oscillation, it has a strong damaging effect on the device. There is still a lack of detailed studies regarding strong pressure oscillation, which is similar to the knock phenomenon in engines. Overall, the effect of a reflected shock wave on the flame propagation and pressure oscillation in the end region of confined space has not been comprehensively discussed.

The present study focuses on turbulent flame propagation controlled by an perforated plate with different hole sizes and porosities in confined space. The interactions between turbulent flame and compression wave including visible shock wave and invisible acoustic wave are investigated. Meanwhile, the different combustion phenomena and relationships of turbulent flame propagation and

pressure oscillation are demonstrated in this work. In this work, a newly designed experimental apparatus equipped with a perforated plate, which employed the technique of fast flame generated by a flame passing through the orifice plate and the theory of self-accelerated turbulent flame, was used. Different intensities of the turbulent flame and shock wave can be generated by effectively controlling the hole sizes and porosities. The interaction between flame front and shock wave was imaged via high-speed Schlieren photography. The effects of a reflected shock wave on the combustion modes and, consequently, on the pressure oscillation were studied in detail. A stoichiometric hydrogen-air mixture was used as the test fuel because of its high flame propagation velocity and the formation of an obvious shock wave ahead of the flame front, which can be used to investigate the interaction of the flame-shock wave. The present study will provide a new insight into not only the knock phenomenon in spark ignition gasoline engines, but also the DDT and pulse detonation phenomenon in engines.

The paper is organized as follows: the experimental setup and conditions are briefly discussed in Section 2. The results and discussion are presented in Section 3, involving the effects of different hole sizes and porosities. In Section 4 the specific combustion modes of normal combustion and reciprocating combustion as well as the analysis of pressure oscillations were shown. Finally, this study's conclusions are presented in the last section.

2. Experimental Setup and Conditions

2.1 Experimental setup

The experiments apparatus is same with our previous study [41], thus the detailed information is not shown here due to the limited length of paper. The experimental apparatus was composed of the constant volume combustion vessel, the orifice plate, the intake and exhaust pipe system, the ignition system, the heating system, time synchronizing system, image acquisition system, and in-cylinder pressure acquisition system.

In the study, two arrangements of the experimental apparatus were applied for different purposes. The schematic of the present experiment was shown in Fig. 1. Setup A: the perforated plate was placed in the middle of the combustion chamber 115 mm away from the right wall, and the spark plug was mounted in the left wall. Thus, the combustion phenomena in the end gas could be observed. Setup B: the perforated plate was mounted 35 mm away from the right wall, and the spark plug was mounted in

the right wall. Note that the position of perforated plate was located at the optical window, which can be used to observe flame acceleration of the laminar flame across the perforated plate. The perforated plate was made using a 3 mm thick stainless steel plate. There were several holes on it depending on the porosity, distributed in rectangular form.

2.2 Experimental conditions

Initially, the combustion chamber was heated up to the target temperature by the temperature control system. The H_2-air mixture was obtained via the partial pressure method. The test conditions are shown in Table 1. Before igniting, the H_2 and air mixture was initially premixed for 2 minutes to achieve a homogeneous mixture at the target condition. After that, the spark igniter, pressure recorder and high-speed digital video camera were triggered simultaneously by the synchronization. In this study, the flame front velocity or tip velocity was calculated based on the time derivation of the flame tip position, distance from the ignition point. A velocity point is calculated from the difference in the centerline flame position between consecutive frames. And this was called flame front velocity in the text. The flame front velocity is an intrinsic property of a premixed flame, which was widely used in the previous study of the flame acceleration and transition to detonation. And a brief review on the flame front velocity could be obtained in our previous study [41]. Based on a framing rate of 160,000 frames per second and a resolution of 0.18 mm/pixel, the uncertainty is 28 m/s.

Table 1. Experimental conditions

Experiment setup	Hole size /mm	Porosity	Equivalence ratio
A/115 mm	1.5	12%	1
	2	12%	
	2.5	12%	
	3	6%	
		12%	
		18%	
		24%	
	4	12%	
	5	12%	
	6	12%	
B/35 mm	3	12%	

2.3 Repeatability test

To verify the repeatability of the test device, three cases of turbulent flame position versus time conducted in setup A under the same conditions (hole size 3 mm, porosity 12%, initial pressure 1 bar) were considered, as shown in Fig. 2. As shown in the figure, the trends of flame trajectory of the three curves are consistent with each other. The relative error does not exceed 5% and is acceptable for high-speed turbulent flame propagation. Thus, the experimental setup in the present study is reliable.

2.4 Definition of flame front velocity

In this study, the flame front velocity was calculated based on the time derivation of the flame tip position, distance from the ignition point. A velocity point is calculated from the difference in the centerline flame position between consecutive frames. In our previous work [41], a detailed investigation regarding the definition of flame front velocity was reviewed.

2.5 The process of flame acceleration

The development of the flame when it passed through the obstacle was demonstrated in Fig. 3. It can be seen that the development of the flame in the present study was divided into three obvious stages: laminar flame propagation, jet flame formation and turbulent flame development. The laminar flame was compressed by the perforated plate and became a flat flame surface, which caused a clearly delayed burning that occurred before the flame passed through the perforated plate. As shown in Fig. 4, the laminar flame front velocity decreased gradually before passing through the perforated plate. Due to the expansion of the burned gas, a flow was formed downstream the flame. After the flow passed through the perforated plate, fast jet flow with a mean velocity of 8 m/s was induced as shown in Fig. 3. And then, the flame was entrained by the fast jet flows through the perforated plate. Driven by the jet flow, the flame accelerated rapidly after passing through the perforated plate. The mean flame front velocity accelerated from 21.8 m/s to 108.2 m/s after passing through the perforated plate. And due to the faster expansion of the burned product, the jet flow gained a faster velocity of 44.3 m/s. As shown in the Fig. 4, during the jet flame stage, the jet flame rapidly after the perforated plate decreased in the terms of the fluid dynamic mechanism that the velocity of a fluid passing through a small space (in orifice plate) with a relatively larger pressure to a large space with relatively smaller pressure will decrease, which is likely the mechanism of Venturi effect. Consequently, the gas flow velocity decreased after the perforated plate according to previous work[41], which contributes to the flame front velocity decrease. Finally, the turbulent flame was formed due to the jet flame merging together through the flame-flame

interaction. Meanwhile, a slight increase of flame front velocity was observed due to the increased flame surface. The present experiment extended the theory previously made by Bychkov[4] from the numerical study and theory analysis. It was noted that in the Bychkov work[4], ultrafast flame acceleration in obstructed channels indicates laminar flame acceleration, but in this work, the jet flame was formed after the laminar flame passed through the perforated plate; subsequently, the turbulent flame was generated. Furthermore, for jet flame formation and development stage, toroidal vortices are generated behind the obstacle at the wake of a circular orifice as the flame passing through the orifice and subsequently the resulting flame-vortex interaction intensifies the rate of flame propagation and the pressure rise, which are clearly demonstrated by the experimental and LES results by Di Sarli [22-24, 26]. In the turbulent flame development, as shown in Fig. 4, the turbulent flame front velocity slightly increased due to the turbulent self-acceleration feature with the wrinkled flame surface[15, 16].

Next, the flame propagation front velocity, shock wave propagation speed, the pressure oscillation and flame-shock interaction were investigated by changing hole size and porosity of the perforated plate.

3 Results and Discussion

3.1 Effect of hole size

Figure 5 shows sequence of photography of flame and shock wave in the end gas of the chamber under conditions of porosity of 12% and initial pressure of 2 bar. The results were obtained through the experimental setup A using perforated plate of different hole sizes. At every hole size, five typical chronological Schlieren images were chosen and listed as a column. Noted that the right edge of each image is the combustion chamber wall. For hole sizes of 2 mm, 2.5 mm, 3 mm, 4 mm and 5 mm, a clear shock wave was observed ahead of the flame front induced by the turbulent flame acceleration. As the hole size increased, the distance between flame front and shock wave decreased, as shown in the first picture of each column. The largest separation between the lead shock wave and the turbulent flame brush occurred for the smallest hole size of 2 mm in this work. When the shock wave reached the end of the combustion chamber, a reflected shock wave appeared. The reflected shock wave can be found from the third-row images in Fig. 5. Regarding the perforated plate with a hole size of 6 mm, no visible shock wave formed ahead of the flame front. However, a reflected shock wave can be observed after the wall reflection at 4.74 ms, owing to the fast turbulent flame in the end region of the confined space, which will be discussed below.

Detailed analysis of the flame-shock wave interaction was carried out for the perforated plate with a hole size of 2 mm as example, as shown in Fig. 5. An obvious shock wave with a speed of approximately 500 m/s was formed ahead of the accelerating turbulent flame at 4.53 ms. After the shock wave reached the end wall in the confined space, an obvious reflected shock wave was generated at 4.58 ms. Subsequently, the clear interaction between flame and reflected shock wave occurred at 4.64 ms. Then the flame front was pushed back and propagated reversely due to the impact of the reflected shock wave and flow field. It was shown that the flame oscillating propagation was observed in the experiment. This can be explained as follows: the flame oscillation is caused by the flow field behind the shock wave as it passes the flame. The shock wave acts as a source of disturbance, leading to velocity change and compression effect on the unburned mixture. This leads to an oscillating combustion in the end region of the combustion chamber, which is the mechanism of flame-shock wave interaction in a confined space. The flame-shock interaction decelerated the flame front velocity and delayed the time when the flame front reached the end wall. Therefore, the end unburned gas would be heated for longer time and more likely to auto-ignite.

Figure 6 shows the flame front velocity as a function of the position in the end region of the combustion chamber equipped with a perforated plate of different hole sizes, under conditions of porosity of 12% and initial pressures of 2 bar. Note that the observation window is located at the end region of the combustion chamber, as shown in Fig. 1. The flame front velocity is calculated from the derivative of the flame front location. The position of 78 mm represents the end wall of the combustion chamber; the zero point represents the flame just entering the observation area at the horizontal axis in Fig. 6. Overall, the flame front velocity increased with the increase of the hole size. At the position of starting point zero, the perforated plate with a hole size of 6 mm had the largest flame front velocity of approximately 450 m/s at an initial pressure of 2 bar. However, the flame front velocity at the hole size of 2 mm was just 75 m/s at an initial pressure of 2 bar. The tendency of the turbulent flame propagation follows the hole size at a constant porosity as shown in Fig. 6. Because flame propagation after the larger hole size leads to produces turbulent vortex with a larger eddy structure. As shown in [22-27], turbulent vortex structures behind the perforated plate were observed as jet flame was generated. In [33], they presented that the vortices could quickly reach the channel top and bottom wall and the vortex zones burn out quicker for the larger hole size or larger space. In the later stage of flame propagation, the larger eddy turbulence could entangle much more unburnt mixture increasing the burning rate and promoting

flame acceleration.

The flame front velocities for perforated plates with large hole sizes of 5 mm and 6 mm decreased in the range of 0 to 30 mm and increased in the range of 30 to 45 mm at an initial pressure of 2 bar in the end region of the confined combustion chamber. Smaller hole sizes of 2 mm, 3 mm and 4 mm showed only an increasing trend before the flame front velocity reduced rapidly at an initial pressure of 2 bar. However, the flame front velocity rapidly decreased in the end-gas region approximately from 45 mm to 78 mm for all the cases. As hole size decreased, the beginning of the flame front velocity drop was advanced. This was consistent with the phenomenon demonstrated in Fig. 5. Meanwhile, as the hole size decreased, the distance between flame front and shock wave increased, as shown in Fig. 4. It was concluded that the flame-shock wave interaction occurred early and the flame front velocity began to reduce in advance. Because of the reverse flow field induced by the reflected shock wave and acoustic wave, the flame front velocity in each case decreased rapidly. For the flame approaching the end of the combustion chamber, the flame front velocity was close to zero and the flame even propagated reversely. Similarly, the strong oscillation in flame front velocity lead by the pressure wave-induced backward and forward flow in confined space was well presented in DNS results by Chen [42] and in experiments by Xiao[11]. Furthermore, a simply 1D simulation is carried out to explain the flame oscillation phenomenon caused by flame-acoustic wave. The relevant results were shown in Appendix A. In the present work, a controlled turbulent flame was generated by changing the hole size of the perforated plate, which is of great help to the investigation of flame acceleration, self-acceleration of turbulent flames and interactions between a flame and shock wave or acoustic wave.

Figure 7 shows the cylinder pressure versus time with different hole sizes, under conditions of porosity of 12% and initial pressure of 2 bar. In the experiment, the pressure transducer (Kistler 6113B at 100 KHz) was mounted on the top wall of the combustion chamber at a distance of 35 mm from the end of the combustion chamber. The upper curves in each subfigure present the original tested cylinder pressure, while the one below shows the pressure high-pass filtered by 20 KHz. The filtered pressure can be used to demonstrate the pressure fluctuation amplitude. As seen from Fig. 7, the peak of the pressure oscillation increases with the increase of hole size and the peak could reach 2.375 MPa at the hole size of 6 mm. This indicates that the intensity of the pressure oscillation is strongly relevant to the turbulent combustion with high turbulent flame front velocity in the end region of the confined combustion chamber. It can also be seen that the high-pressure oscillation also has high oscillation

frequency.

Figure 8 shows the shock wave velocity with the perforated plate of different hole sizes and under conditions of porosity of 12% and initial pressure of 2 bar. Note that the positive values represent the forward propagating shock wave and the negative ones show the shock wave reflected by the end wall of the combustion chamber. Briefly, as shown in Fig. 8, the forward propagating shock waves maintained their velocity at approximately 500-600 m/s and there was no significant difference as the hole sizes varied. Note that the forward propagating shock wave was not formed at the large hole size of 6 mm.

However, apparent differences for the reflected shock wave evolution among the hole sizes were observed, as shown in Fig. 8. After reflection, the shock wave had a similar velocity of approximately 480 m/s at the position of 74 mm. With the propagation of the reflected shock wave, the differences between shock wave velocities appeared for different hole sizes. Note that the reflected shock wave decays faster with larger hole size. This phenomenon is opposite to the trend of flame front velocity in Fig. 6 in the end region of the combustion chamber. This is because the reflected shock wave and the turbulent flame in the end region of the chamber have opposite propagating directions. The relationship of mutual inhibition competition will occur between them. The turbulent flame weakened the reflected shock waves; thus, reflected shock waves prevented the turbulent flame propagation. Therefore, in the turbulent flame-shock interactions, the reflected shock wave velocity reduced due to the flow ahead of the flame. As the shock wave passed through the flame, the flame was pushed back. And due to R-M instability, the turbulent flame surface increased and accelerated after the shock wave passed by. The phenomenon was obviously observed in the present experiment.

3.2 Effect of porosity

Figure 9 shows sequence of photography of the flame and shock wave in the end region of the chamber equipped with a perforated plate of different porosities. The experiments were carried out under conditions of hole size of 3 mm and initial pressure of 3 bar. It can be seen that a shock wave was generated ahead of the turbulent flame front at porosities of 6% and 12%. At the porosity of 6%, there were several compression waves ahead of the flame shown by the Schlieren photography. This is caused by the strong acceleration effects. The turbulent flame interacted with the shock reflected from the end wall and the shock-flame interactions further distorted and wrinkled the flame based on the RM instability, which also enhanced the small-scale turbulence and the surface area of the flame and

consequently increased the energy release rate in the combustion chamber. By comparing the timing of the turbulent flame entering the observation window as shown in Fig. 9, an earlier timing was found for the smaller porosity. Note that the bright zone observed in Fig. 9 is located at the burnt regime, and it should be as a strong burning because of no significant pressure increase, and flame acceleration and propagation, which is not similar to our previous work regarding autoignition with the flame acceleration and very high pressure oscillation[43].

It can also be concluded that for a smaller porosity, the flame front configuration or flamelet can be clearly distinguished, particularly at the porosity of 6%. Note that Fig. 9 not only indicates the flame-shock interaction but also demonstrates the flame-acoustic interaction clearly. There were many studies regarding the flame-acoustic interaction based on theory, numerical and experimental methods[11, 18]. For these studies, the flame is mostly the laminar flame. However, the turbulent flame-acoustic interaction was clearly demonstrated by the present experiment at the porosity of 24%. The flame front velocity began decreasing at t=5.02 ms in Fig. 8. The flame front only moved forward a little distance for approximately 0.2 ms from 5.02 ms to 5.23 ms. However, the flame did not move forward first and slightly moved backward, which was observed from 5.23 ms to 5.38 ms. Subsequently, the flame accelerated and moved forward at a relatively small velocity again. Finally, a second backward motion of the flame was observed at approximately 5.65 ms. Note that an obvious flame front was generated at 5.65 ms. This is possibly because the flame front velocity is very low, and the combustion at the burnt region behind the flame front has enough time to finish. Consequently, the fuel-air mixture has been fully consumed sufficiently far from the flame front for 24% porosity. After the flame-acoustic interaction, the turbulent front became more complicated again at 6.73 ms. The evolution of the flame front velocity involving the flame-acoustic interaction is discussed later.

It can be concluded from Figs. 5 and 9 that the present experiments could yield both the turbulent flame-shock interaction and turbulent flame-acoustic or pressure wave interaction by controlling the perforated plate parameters.

Figure 10 shows the flame front position versus time in the end region of the combustion chamber with a perforated plate of various porosities, under conditions of hole size of 3 mm, initial pressure of 3 bar. As shown in Fig. 10, the smaller the porosity, the more advanced the flame that enters the observation window. The gradient of position versus time for smaller porosity indicates that it could

generate a faster flame front velocity. At the initial stage, the evolution of the flame front position is approximately linear with time. This indicates that the flame front velocity retained relatively constant. In the later stage, an oscillating propagation of the flame was formed due to the impact of the shock wave or pressure wave. Note that with the increase of porosity, flame pulsation occurs in advance and the oscillation frequency increases. The flame front velocity evolutions with various porosities are presented in Fig.11

Figure 11 shows the flame front velocity versus time in the end region of the combustion chamber equipped with a perforated plate of different porosities. The experiments were carried out at conditions of hole size of 3 mm and initial pressure of 3 bar. It can be concluded that the flame front velocity increases as the porosity decreases. At the beginning stage of the flame entering the observation window, the flame front velocity maintained constant velocity for four porosities, which was consistent with the results shown in Fig. 10. Meanwhile, the perforated plate with the smallest porosity of 6% had the largest flame front velocity (roughly 400 m/s) at initial pressure of 3 bar. The flame front velocity for a porosity of 24% was just 180 m/s. As the flame entered the region near the end wall, flame front velocity began to reduce rapidly. As porosity increased, the onset of the decrease of flame front velocity moved forward. The phenomenon is also clearly demonstrated in Fig. 10. As the porosity increases, the transmittance of the perforated plate increases. This allows intense flow and heat exchange between two sides of the perforated plate. Consequently, the flame velocities for smaller porosities were relatively larger. Thus, the beginning location at which the flame front velocity starts declining moved towards the end wall for small porosities. Actually, the present work is not different from the previous studies[7], in which the magnitude of shock and flame centerline velocity in tests with larger obstacles was lower than that with smaller obstacles. The possible explanation for the present work is that the small porosity may induce a strong jet flame at a constant hole size due to much confined effect on the initial turbulent formation. Meanwhile, the small eddy turbulence forms early. In this situation, the limited effect and small eddy turbulence become noticeable and control the turbulent flame acceleration. The conclusion is consistent with the theory analysis[44]. Moreover, the smaller porosity means the much more holes in perforated plate and could produce more turbulent vortex structures behind the perforated plate as jet flame is generated. The works focused on the transient flame-turbulence/vortex interaction by Di Sarli[22-27] can prove that the turbulent vortex distorts the flame and subsequently increases the flame surface area and burning rate. Note that the high rate of pressure rise occurs due to the intense turbulent combustion,

which will be discussed later.

Figure 12 shows the cylinder pressure under conditions of hole size of 3 mm and initial pressure of 3 bar. The pressure transducer was located on the top wall at a distance of 35 mm to the right wall. As shown in Fig. 12, the peak value of the pressure decreased as porosity increased; the peak value was up to 2.7 MPa for a porosity of 6%. Similarly, the amplitude of the pressure oscillation also decreased as porosity increased and the beginning of pressure oscillation occurred earlier with the decrease of porosity. This suggests that the smaller the porosity, the greater the turbulent combustion. This increased the flame front velocity in the end region of the combustion chamber, i.e., the burning rate increased. Therefore, the peak value and the amplitude of the pressure for small porosity were larger than those for large porosity. Note that for the porosity of 24% with the flame-acoustic wave or compression wave, flame-acoustic resonance was not observed in this work because of the complex turbulent combustion with complicated pressure waves from different directions in the confined space. Referring to the turbulent flame evolution images in Fig. 9, the rising timing of pressure followed the arrival of the turbulent flame and compression wave; subsequently, the pressure oscillation was controlled by the turbulent combustion and its interaction with the pressure wave or shock wave. The experiment showed that turbulent flame-shock interactions and strong turbulent combustion resulted in a strong pressure oscillation. The present pressure oscillation amplitude generated by the turbulent combustion in the present small confined space is greater than that which occurred in the tube with porous media[45].

Figure 13 shows the shock wave velocity as a function of position under conditions of hole size of 3 mm and initial pressure of 3 bar. Note that in this work the shock wave was generated at only two smaller porosities due to larger turbulent flame front velocity, as shown in Fig. 9. It can be seen that when the porosity of the perforated plate was up to 12%, the incident shock wave was observed first at the position of 14 mm and the shock velocity was approximately 590 m/s. For a porosity of 6%, the velocity of the incident shock wave was slightly smaller (approximately 500 m/s) and was observed later (at 45 mm). The forward propagating shock wave was not formed at larger porosities of 18% and 24%. After reflection, the reflected shock velocities of porosities of 6% and 12% were 400 m/s and 450 m/s at 75 mm, respectively. With the development of the reflected shock wave, the velocity of the reflected shock decayed to 300 m/s. As mentioned above, the velocity of reflected shock wave was strongly related to the turbulent flame front velocity. Therefore, the velocity of the reflected shock wave at a porosity of 6% was smaller than that at a porosity of 12%. Note that the turbulent flame-shock wave

interactions become important for the turbulent flame propagation and unburned mixture thermodynamic states in the end region of the confined space, which may induce the end-gas autoignition at a certain condition.

4. Flame-shock wave interaction-oscillating combustion

Figure 14 illustrates sequence of photography of flame and shock wave in the end region of the combustion region under the conditions of hole size of 2.5 mm, porosity of 12% and initial pressure of 3 bar. An obvious shock wave with a speed of approximately 500 m/s was observed ahead of the accelerating turbulent flame, as shown in Fig. 14 at 4.775 ms. As the shock wave reached the end wall of the combustion chamber at approximately 4.806 ms, as shown in Fig. 14, a reflected shock wave was clearly generated at 4.825 ms. The reflected shock wave touched the turbulent flame at 4.888 ms and there were some disturbance waves behind the reflected shock. Consequently, the flame front was pushed back and spread reversely at 5.063 ms. Thus, the oscillating velocity of the turbulent flame was generated in the end gas region. Based on Taylor instability theory, Markstein[46] suggested that this flame inversion is caused by the velocity field (drastic velocity decrease) behind the shock wave as it passes the flame. A drastic change in the unburned gas velocity is produced by the shock wave effect, causing violent velocity decrease and reverse flow in the unburned region. The shock wave acts as a source of disturbance, leading to velocity change in the unburned mixture.

Shown in Fig. 15 are flame front trajectory, shock wave trajectory and pressure oscillation under conditions of hole size of 2.5 mm, porosity of 12%, and initial pressure of 3 bar. The velocities of the shock wave and flame versus time are plotted in Fig. 16. As shown, the trajectory of flame propagation is related to the trajectory of shock wave development. It can be found that the relationship of the location of the forward shock wave with a velocity of approximately 550 m/s and time was almost linear. For the shock reflection, the velocity of the reflected shock was reduced to approximately 460 m/s and then decreased with time as shown in Fig. 16. This is because the reflected shock wave is hindered by the gas compression effect induced by flame acceleration in front of the accelerating turbulent flame. Note that the flame-shock interaction makes the velocity decrease for both the shock wave and turbulent flame. The reflected shock velocity slowed down to approximately 290 m/s as it contacted the flame front at point D, as shown in Fig. 15. The relationship between pressure oscillation and shock wave is also presented in Fig. 15. It was found that the two peaks of pressure oscillation tested by the pressure

transducer at the two points A and C in Fig. 15 were induced by the shock wave.

As the flame and shock wave interaction occurred, the leading reflected shock further pushed the turbulent flame brush back decreasing the flame front velocity; subsequently, the flame moved backward due to the effect of a series of distorted compression waves, as shown in Fig. 16. Note that the negative flame front velocity indicated that the flame propagates reversely because the reflected shock wave was strong enough to push the flame back. During the flame-shock interaction, a pressure oscillation with maximum amplitude of 1.3 MPa was generated. After that, turbulent flame front velocity began to increase, with the wrinkled flame surface increasing the flame surface area. As comparison to the oscillating combustion, the normal combustion phenomenon can be found in Supplemental material.

5. Conclusions

In this work, the phenomenon of turbulent flame formation, pressure oscillation and flame-shock interactions for different parameters was comprehensively investigated in a newly designed confined chamber equipped with a perforated plate. The interaction of flame front and shock wave was imaged via high-speed Schlieren photography. In this work, three types of flame propagation including laminar flame, jet flame and turbulent flame, were observed. The different propagation speeds of the turbulent flame and shock wave could be obtained by controlling the hole sizes and porosities.

According to the current study, a controlled turbulent flame can be generated in our experiments. The intensity of flame front velocity and pressure oscillation depends on the hole size and porosities of the perforated plate. As the hole size increases, the distance between flame front and shock wave decreases. Meanwhile, the flame front velocity increases as the hole size increases. However, as hole size decreases, the beginning of flame front velocity reduce is advanced. The intensities of pressure oscillation and the reflected shock wave are related to the combustion intensity or flame front velocity. The shock reflection intensity is the opposite of the turbulent flame front velocity. In fact, the flame front velocity in the end region of a confined space in this work is strongly related to two competing effects: the initial turbulent formation due to confined effects and turbulent flame development with larger eddy turbulence. A more in-depth study will be carried out in our future work.

The experiments suggest that an oscillating flame is associated with both the reflected shock wave and the acoustic wave. For the case without a visible shock wave, the flame front velocity also oscillates

in the end gas region and the velocity reduces rapidly as the flame enters the observation window. Note that the flame oscillation was caused by the acoustic wave. However, an apparent flame-shock wave interaction can be found in this work. An obvious shock wave with a speed of approximately 500 m/s formed ahead of the accelerating turbulent flame. Meanwhile, the relationships of flame front velocity, pressure oscillation and shock wave were clearly demonstrated by the present experiment.

In summary, it can be concluded that the pressure oscillation in a combustion chamber is determined by the turbulent flame front velocity in the end region in the present work. In the newly designed experiment, three different turbulent flame propagation and combustion modes were observed by changing the hole size and porosity of the perforated plate: the weak pulsation propagation of a turbulent flame due to the flame-acoustic wave interactions, the pulsation propagation of a turbulent flame with a reflected shock wave, and the strong pulsation propagation of a turbulent flame with backward propagation with a reflected shock wave.

Acknowledgments

The work is supported by The Major Program of the National Natural Science Foundation of China (Grant No. 91641203) and National Natural Science Foundation of China (Grant No. 91741119, 51476114). We also thank the reviewers for providing helpful comments and suggestions.

Appendix A：Flame/Flow-Acoustic/Shock Wave Interactions

A1 Model setup

The objective of this section is to simply explain the experimental results in the present work. Therefore, A one dimension (1D) simulation of flame/flow-acoustic/shock wave interaction in a closed chamber has been carried out, with detailed chemistry and transport of H_2-O_2-Ar mixture. And three cases with different initial conditions are investigated in present work, where nonreacting flow-shock wave, flame-acoustic wave and flame-shock wave are involved. Taking the case of flame-acoustic wave as an example to introduce the computational domain here, is shown in Fig. A1. The domain is divided into two parts, initialization zone and propagation zone. In this case, the initial pressure is uniformly distributed in the whole domain. The initial temperature is uniformly distributed in the propagation zone while it is linearly distributed from 1800 K to 300 K in the initialization zone. And the initial flow velocity is zero everywhere. Both the right and left boundary conditions are reflective. The flame is initialized by the hot kernel in the initialization zone and propagates towards the right boundary. It should be noted that different initial distributions in pressure and temperature in the domain are adopted in order to lead to different phenomena, and the detailed setup is listed in Table.A1. The similar model setup can be found in [47-48]

Table A1. Initial conditions of different cases

Cases	Temperature(K)		Pressure(atm)		Mole fraction	Chamber Length(cm)
	Initialization	Propagation	Initialization	Propagation		
1.Non-reacting flow-shock	300	300	7	0.3	Pure Ar	4
2.Flame-shock wave	1800, uniformly	300	1,3	1	H_2:O_2:Ar 2:1:3.76	4
3.Flame-acoustic wave	1800-300, linearly	300	0.7	0.7		3

A2 Numerical methodology

The program AMROC (Adaptive Mesh Refinement in Object-oriented C++), a freely available dimension-independent mesh adaptation framework for time-explicit Cartesian finite volume methods on distributed memory machines[49], is utilized in this work, with unsteady reactive compressible NS equations as governing equations. The hydrodynamic solution process in AMROC is divided into the two steps of numerical flux calculation and reconstruction. And the first-order accurate Godunov splitting is adopted to decouple the stiff reaction terms and hydrodynamic transport numerically. A hybrid Roe-HLL Riemann solver is used to construct the inter-cell numerical upwind fluxes while the Minmod limiter with MUSCL reconstruction is applied to construct a second-order method in space. The MUSCL-Hancock technique is adopted for second-order accurate time integration. Moreover, the adaptive mesh refinement is used to guarantee adequate numerical resolutions for the propagating flame front and waves. And the max level is five with the finest mesh of 10 μm.

A3 Case 1

In the case of nonreacting flow-shock wave, the pressure, density and flow velocity are tracked at the position of 2.5 cm (called monitoring point in the following), and the time histories of these quantities are shown in Fig. A2. As can be seen, when the shock arrives at the monitoring point from left to right at about 40 μs, there is abrupt increase in all the pressure, density and flow velocity. Especially, the flow velocity reaches up to nearly 300 m/s while the initial value is 0 m/s. Then they decrease gradually as the shock leaves the point. After the shock reflects at the right boundary, it passes through the monitoring point again at 104 μs, which makes the density and pressure increase and reverses the flow velocity. It should be noted that the reflected shock wave is weaker than before, because the amplitudes of the pressure and density rise are both smaller than that at the first time as well as flow velocity.

A4 Case 2

In the case of flame-shock wave, the shock wave can be seen after the flame starts to propagate from left to right, as shown in Fig. A3. And the flame is not coupled with the shock wave, because the velocity of latter is much faster than that of the former. Then the shock wave reflects at the right boundary (from line#3 to line #4) and moves forward to the flame rapidly. Eventually, the shock wave comes into contact with the flame at 192μs (line #6), and even pushes the flame backwards from line#6 to line#7. After that, the shock wave reflects once more at the left boundary and catches up with the

flame (line#8). They meet each other again and again when the flame propagates to the right boundary, which causes the oscillation of the flame velocity, as shown in Fig. A4. In this work, the flame front X_f is defined as the position with local peak heat release rate and the flame speed is $S=dX_f/dt$. The oscillation of the flame velocity is because that the velocity of flow where the flame locates is influenced by the shock wave as discussed in case 1. It can be further confirmed in Fig. A4, which shows that the oscillation tendency of flame front velocity is almost consistent with that of flow velocity. The maximum oscillation amplitude of flame speed is 102 m/s. In addition, the burning velocity is generally increased because the temperature rises in the chamber. Note that , there are several different ways to define the turbulent burning velocity, as described in detail in [48]. Here, we simply use the third method (V_{flame}-V_{gas}) in [50] in present 1D simulation.

When initial pressure is 3 bar in the initialization zone and propagation zone is at 1 bar, the shock wave can be much stronger, which makes the oscillation amplitude of flame front velocity higher, up to 145 m/s, as shown in Fig. A5. And the increasing burning velocity is also observed in this case.

When the initial pressure is decreased from 1 bar to 0.7 bar, the initial shock wave wakens to the acoustic wave in the case 3, as shown in Fig. A6. Although similarly to the flame-shock wave interaction, the acoustic wave moves backward and forward in the chamber and causes the flame oscillation, the amplitude is much lower, only 37 m/s, as shown in Fig. A7. And the burning velocity is also increasing with oscillation in this case.

A5 Case 3

In conclusion, the pressure wave moves backward and forward, which causes the oscillation of the flame front velocity. And the pressure waves motion results from the velocity of flow where the flame locates is influenced by the wave. And the stronger the wave is, the greater the amplitude of oscillation is. In addition, the burning velocity is increased with oscillation when the flame propagates from left to right.

Appendix B：Comparison of experimental and theoretical values

The initial conditions for the test are p1 (absolute pressure) =300000 Pa, T1 (temperature) =373 K, γ (assumed adiabatic index) =1.4. The absolute pressure after shock wave p2= 800000 Pa, which is shown in figure 15. Among them, the subscript 1 and 2 indicate the gas state parameters ahead of and after the shock wave respectively.

According to the ideal gas state equation,

$$\rho_1 = \frac{p_1}{RT_1} = 2.8 \text{ kg/m}^3$$

According to Rankine-Hugoniot equation,

$$\frac{\rho_1}{\rho_2} = \frac{\frac{\gamma+1}{\gamma-1}\frac{p_2}{p_1}+1}{\frac{\gamma+1}{\gamma-1}+\frac{p_2}{p_1}} = 1.96$$

Thus,

$$\rho_2 = 1.96\rho_1 = 5.488 \text{ kg/m}^3$$

According to the temperature relationship,

$$\frac{T_2}{T_1} = \frac{\frac{\gamma+1}{\gamma-1}\frac{p_2}{p_1}+(\frac{p_2}{p_1})^2}{\frac{\gamma+1}{\gamma-1}\frac{p_2}{p_1}+1} = 1.36$$

Thus,

$$T_2 = 1.36T_1 = 507.28 \text{ K}$$

$$v_s = \sqrt{\frac{p_2-p_1}{\rho_2-\rho_1}\cdot\frac{\rho_2}{\rho_1}} = 603.8 \text{ m/s}$$

Where v_s is the calculated shock wave propagation speed. As shown in Fig. 16, the measured shock wave propagation speed is about 550 m/s. It shows that the calculated value is reliable. The temperature after shock wave is about 507.28 K.

References

[1] Z. Jozefik, A.R. Kerstein, H. Schmidt, Simulation of shock–turbulence interaction in non-reactive flow and in turbulent deflagration and detonation regimes using one-dimensional turbulence, Combust. Flame 164 (2016) 53-67.

[2] L.D. Landau, E.M. Lifshitz, Fluid mechanics, Elsevier1987.

[3] B. Hof, C.W. van Doorne, J. Westerweel, F.T. Nieuwstadt, Turbulence regeneration in pipe flow at moderate Reynolds numbers, Phys Rev Lett 95 (2005) 214502.

[4] V. Bychkov, D. Valiev, L.-E. Eriksson, Physical mechanism of ultrafast flame acceleration, Phys Rev Lett 101 (2008) 164501.

[5] S. Chaudhuri, F. Wu, D. Zhu, C.K. Law, Flame speed and self-similar propagation of expanding turbulent premixed flames, Phys Rev Lett 108 (2012) 044503.

[6] E.S. Oran, V.N. Gamezo, Origins of the deflagration-to-detonation transition in gas-phase combustion, Combust. Flame 148 (2007) 4-47.

[7] G. Ciccarelli, C.T. Johansen, M. Parravani, The role of shock–flame interactions on flame acceleration in an obstacle laden channel, Combust. Flame 157 (2010) 2125-2136.

[8] G. Ciccarelli, S. Dorofeev, Flame acceleration and transition to detonation in ducts, Prog Energ Combust 34 (2008) 499-550.

[9] S.B. Dorofeev, Flame acceleration and explosion safety applications, Proc Combust Inst 33 (2011) 2161-2175.

[10] G. Roy, S. Frolov, A. Borisov, D. Netzer, Pulse detonation propulsion: challenges, current status, and future perspective, Prog Energ Combust 30 (2004) 545-672.

[11] H. Xiao, X. Shen, S. Guo, J. Sun, An experimental study of distorted tulip flame formation in a closed duct, Combust. Flame 160 (2013) 1725-1728.

[12] L. Maley, R. Bhattacharjee, S.-M. Lau-Chapdelaine, M.I. Radulescu, Influence of hydrodynamic instabilities on the propagation mechanism of fast flames, Proc Combust Inst 35 (2015) 2117-2126.

[13] M.I. Radulescu, B.M. Maxwell, The mechanism of detonation attenuation by a porous medium and its subsequent re-initiation, J. Fluid Mech. 667 (2011) 96-134.

[14] D.M. Valiev, V.y. Akkerman, M. Kuznetsov, L.-E. Eriksson, C.K. Law, V. Bychkov, Influence of gas compression on flame acceleration in the early stage of burning in tubes, Combust. Flame 160 (2013) 97-111.

[15] D. Bradley, C. Sheppart, R. Woolley, D. Greenhalgh, R. Lockett, The development and structure of flame instabilities and cellularity at low Markstein numbers in explosions, Combust. Flame 122 (2000) 195-209.

[16] F. Wu, G. Jomaas, C.K. Law, An experimental investigation on self-acceleration of cellular spherical flames, Proc Combust Inst 34 (2013) 937-945.

[17] V.N. Gamezo, A.M. Khokhlov, E.S. Oran, Effects of wakes on shock-flame interactions and deflagration-to-detonation transition, Proc Combust Inst 29 (2002) 2803-2808.

[18] A. Petchenko, V. Bychkov, V. Akkerman, L.-E. Eriksson, Violent folding of a flame front in a flame-

acoustic resonance, Phys Rev Lett 97 (2006) 164501.

[19] A. Petchenko, V. Bychkov, V. Akkerman, L.-E. Eriksson, Flame–sound interaction in tubes with nonslip walls, Combust. Flame 149 (2007) 418-434.

[20] T. Lieuwen, Analysis of acoustic wave interactions with turbulent premixed flames, Proc Combust Inst 29 (2002) 1817-1824.

[21] V.N. Gamezo, A.M. Khokhlov, E.S. Oran, The influence of shock bifurcations on shock-flame interactions and DDT, Combust. Flame 126 (2001) 1810-1826.

[22] V. Di Sarli, A. Di Benedetto, E.J. Long, G.K. Hargrave, Time-Resolved Particle Image Velocimetry of dynamic interactions between hydrogen-enriched methane/air premixed flames and toroidal vortex structures, Int. J. Hydrogen Energy 37 (2012) 16201-16213.

[23] V. Di Sarli, A. Di Benedetto, Effects of non-equidiffusion on unsteady propagation of hydrogen-enriched methane/air premixed flames, Int. J. Hydrogen Energy 38 (2013) 7510-7518.

[24] V. Di Sarli, A. Di Benedetto, G. Russo, Large Eddy Simulation of transient premixed flame–vortex interactions in gas explosions, Chem. Eng. Sci. 71 (2012) 539-551.

[25] V. Di Sarli, A. Di Benedetto, G. Russo, Sub-grid scale combustion models for large eddy simulation of unsteady premixed flame propagation around obstacles, J. Hazard. Mater. 180 (2010) 71-78.

[26] V. Di Sarli, A. Di Benedetto, G. Russo, S. Jarvis, E.J. Long, G.K. Hargrave, Large Eddy Simulation and PIV Measurements of Unsteady Premixed Flames Accelerated by Obstacles, Flow Turbul Combust 83 (2009) 227-250.

[27] V. Di Sarli, A.D. Benedetto, Sensitivity to the presence of the combustion submodel for large eddy simulation of transient premixed flame–vortex interactions, Ind Eng Chem Res 51 (2012) 7704-7712.

[28] A.M. Na'inna, G.B. Somuano, H.N. Phylaktou, G.E. Andrews, Flame acceleration in tube explosions with up to three flat-bar obstacles with variable obstacle separation distance, J. Loss Prev. Process Indust. 38 (2015) 119-124.

[29] S. Maeda, S. Minami, D. Okamoto, T. Obara, Visualization of deflagration-to-detonation transitions in a channel with repeated obstacles using a hydrogen–oxygen mixture, Shock Waves 26 (2016) 573-586.

[30] G. Ciccarelli, C.J. Fowler, M. Bardon, Effect of obstacle size and spacing on the initial stage of flame acceleration in a rough tube, Shock Waves 14 (2005) 161-166.

[31] G. Ciccarelli, B.D. Witt, Detonation Initiation by Shock Reflection from an Orifice Plate, Shock Waves 15 (2006) 259-265.

[32] T. Pinos, G. Ciccarelli, Combustion wave propagation through a bank of cross-flow cylinders, Combust. Flame 162 (2015) 3254-3262.

[33] C.T. Johansen, G. Ciccarelli, Visualization of the unburned gas flow field ahead of an accelerating flame in an obstructed square channel, Combust. Flame 156 (2009) 405-416.

[34] R. Hall, A. Masri, P. Yaroshchyk, S. Ibrahim, Effects of position and frequency of obstacles on turbulent premixed propagating flames, Combust. Flame 156 (2009) 439-446.

[35] A. Masri, A. AlHarbi, S. Meares, S. Ibrahim, A comparative study of turbulent premixed flames propagating past repeated obstacles, Ind Eng Chem Res 51 (2012) 7690-7703.

[36] S. Maeda, S. Minami, D. Okamoto, T. Obara, Visualization of deflagration-to-detonation transitions in a channel with repeated obstacles using a hydrogen–oxygen mixture, Shock Waves 26 (2016) 1-14.

[37] D. Valiev, V. Bychkov, V.y. Akkerman, C.K. Law, L.-E. Eriksson, Flame acceleration in channels with obstacles in the deflagration-to-detonation transition, Combust. Flame 157 (2010) 1012-1021.

[38] V.N. Gamezo, T. Ogawa, E.S. Oran, Deflagration-to-detonation transition in H2-air mixtures: Effect of blockage ratio, AIAA Paper 440 (2009) 5-8.

[39] G.B. Goodwin, R.W. Houim, E.S. Oran, Effect of decreasing blockage ratio on DDT in small channels with obstacles, Combust. Flame 173 (2016) 16-26.

[40] G. Thomas, R. Bambrey, C. Brown, Experimental observations of flame acceleration and transition to detonation following shock-flame interaction, Combust Theor Model 5 (2001) 573-594.

[41] H. Wei, J. Zhao, L. Zhou, D. Gao, Z. Xu, Effects of the equivalence ratio on turbulent flame–shock interactions in a confined space, Combust. Flame 186 (2017) 247-262.

[42] H. Yu, Z. Chen, End-gas autoignition and detonation development in a closed chamber, Combust. Flame 162 (2015) 4102-4111.

[43] H. Wei, D. Gao, L. Zhou, J. Zhao, R. Chen, Experimental Investigation of Turbulent Flame Propagation and Pressure Oscillation in a Constant Volume Chamber Equipped With an Orifice Plate, Combust. Sci. Technol., doi:10.1080/00102202.2017.1389910(2017) 1-17.

[44] D. Valiev, V. Bychkov, V.Y. Akkerman, C.K. Law, L.E. Eriksson, Flame acceleration in channels with obstacles in the deflagration-to-detonation transition, Combust. Flame 157 (2010) 1066-1079.

[45] G. Ciccarelli, C. Johansen, M. Kellenberger, High-speed flames and DDT in very rough-walled channels, Combust. Flame 160 (2013) 204-211.

[46] G.H. Markstein, A shock-tube study of flame front-pressure wave interaction, Symposium on Combustion 6 (1957) 387-398.

[47] P. Dai, Z. Chen, Supersonic reaction front propagation initiated by a hot spot in n-heptane/air mixture with multistage ignition, Combust. Flame 162 (2015) 4183-4193.

[48] C. Qi, P. Dai, H. Yu, Z. Chen, Different modes of reaction front propagation in n-heptane/air mixture with concentration non-uniformity, Proc Combust Inst 36 (2017) 3633-3641.

[49] Ralf Deiterding. Block-structured adaptive mesh refinement-theory,implementation and application.ESAIM:Proceedings,2011,1-10

[50] J.F. Driscoll , Turbulent premixed combustion: flamelet structure and its effect on turbulent burning velocities, Prog. Energy Combust. 34 (2008) 91–134

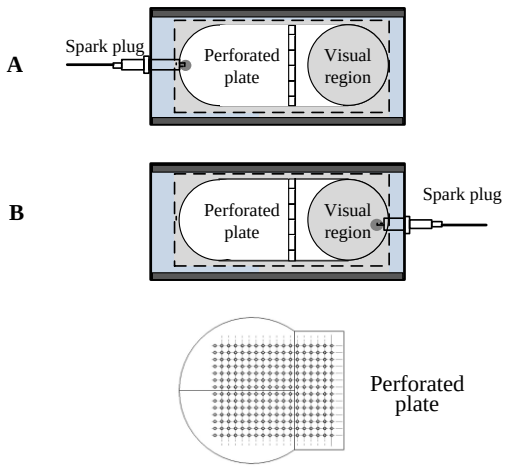

Fig.1 Schematic of experiment including perforated plate

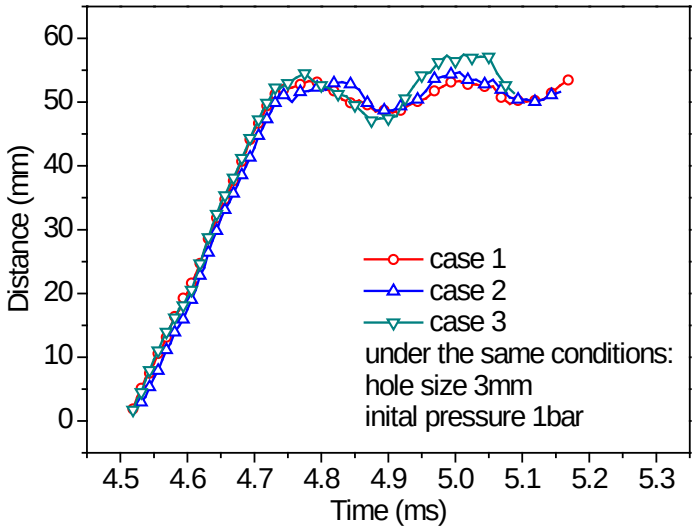

Fig. 2 Repeatability test

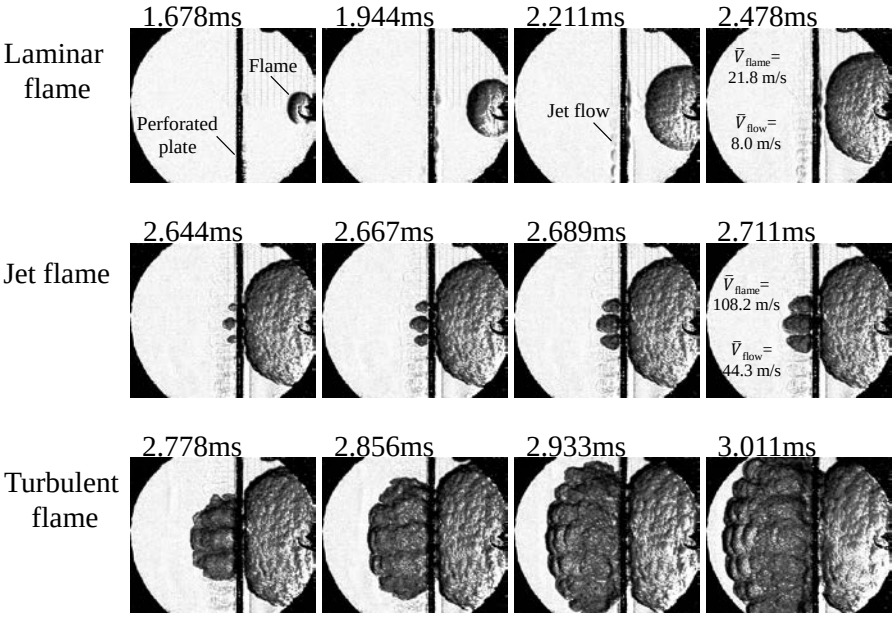

Fig. 3 Process of flame passing through perforated plate under conditions of hole size of 3 mm, porosity of 12% and initial pressure of 3 bar based on experimental setup B

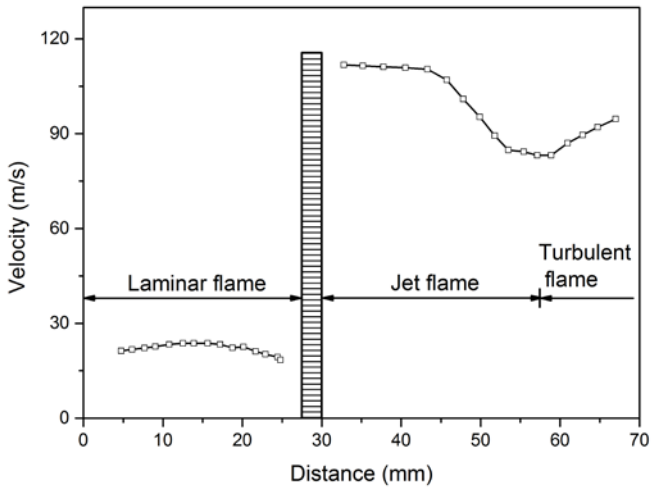

Fig. 4 Flame front velocity versus distance

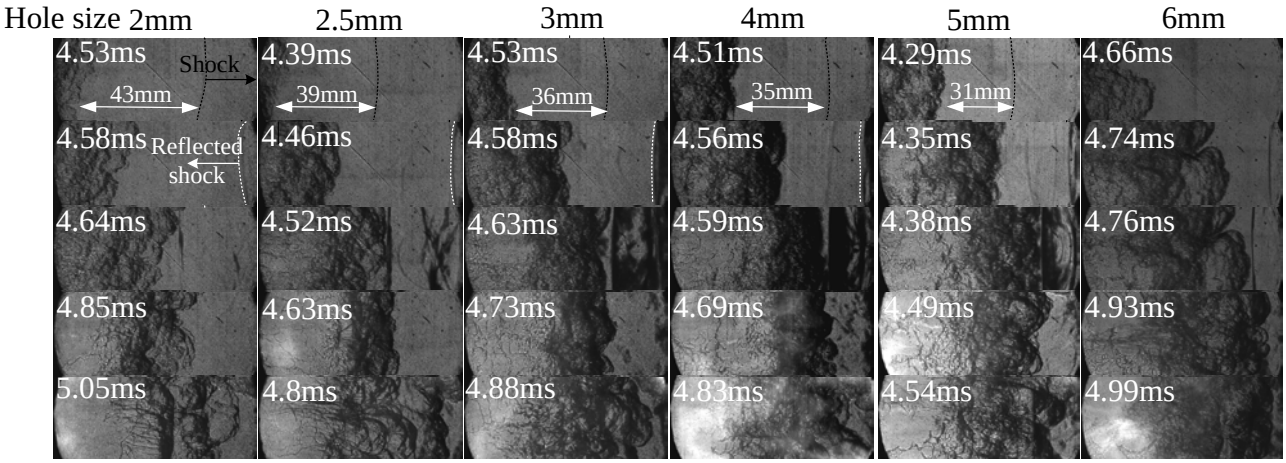

Fig.5 Sequence of photography of flame and shock wave with different hole sizes, under conditions of porosity of 12% and initial pressure of 2 bar based on experimental setup A

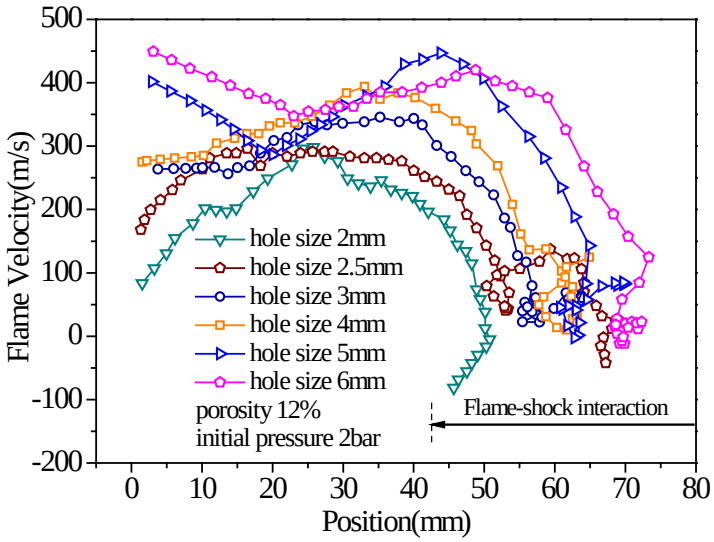

Fig. 6 Flame front velocity with different hole sizes, under conditions of porosity of 12%, initial pressures of 2 bar based on experimental setup A

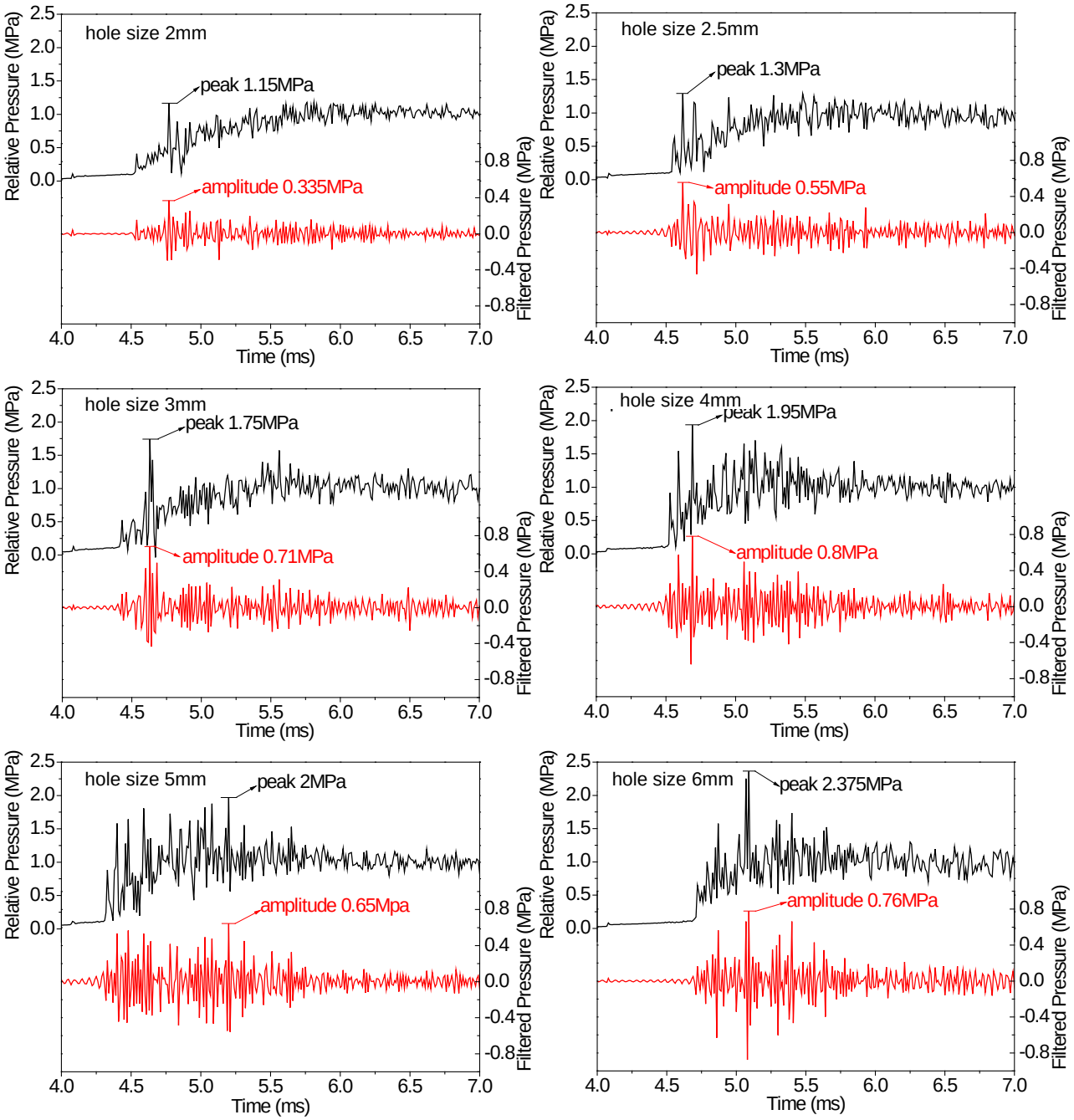

Fig. 7 Cylinder pressure with different hole sizes, under conditions of porosity of 12%, initial pressure of 2 bar based on experimental setup A

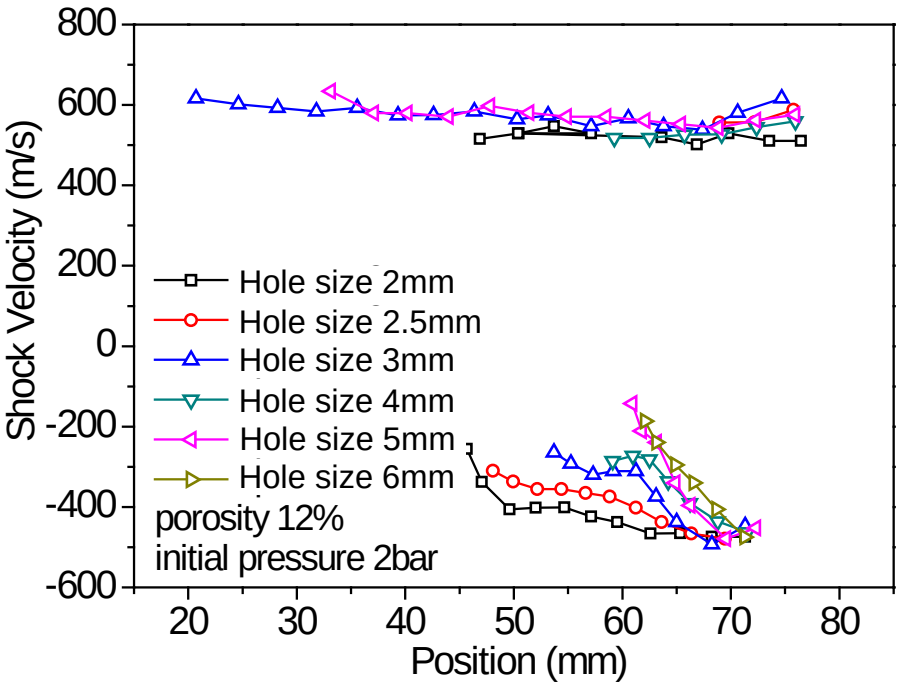

Fig. 8 Shock velocity with different hole sizes, under conditions of porosity of 12% and initial pressure of 2 bar based on experimental setup A

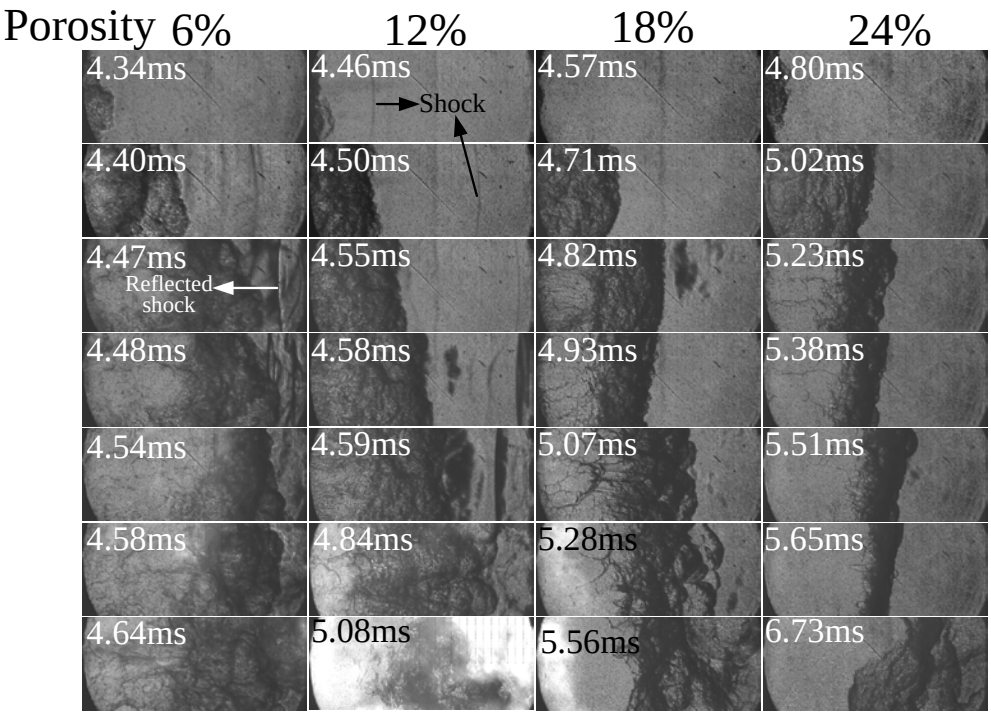

Fig. 9 Sequence of photography of flame and shock wave at different porosities, under conditions of hole size of 3 mm and initial pressure of 3 bar based on experimental setup A

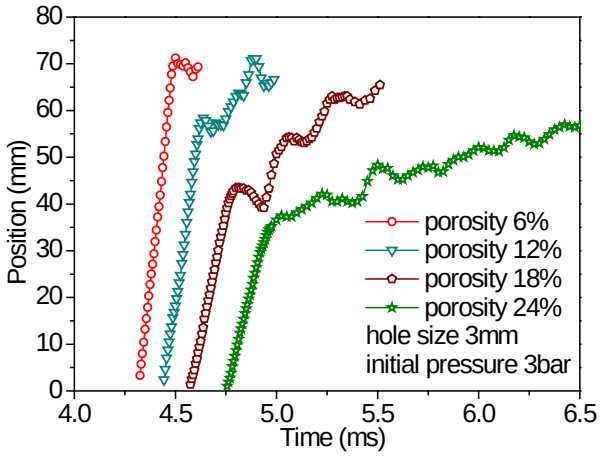

Fig. 10 Flame front position versus time at different porosities, under conditions of hole size of 3 mm, initial pressure of 3 bar based on experimental setup A

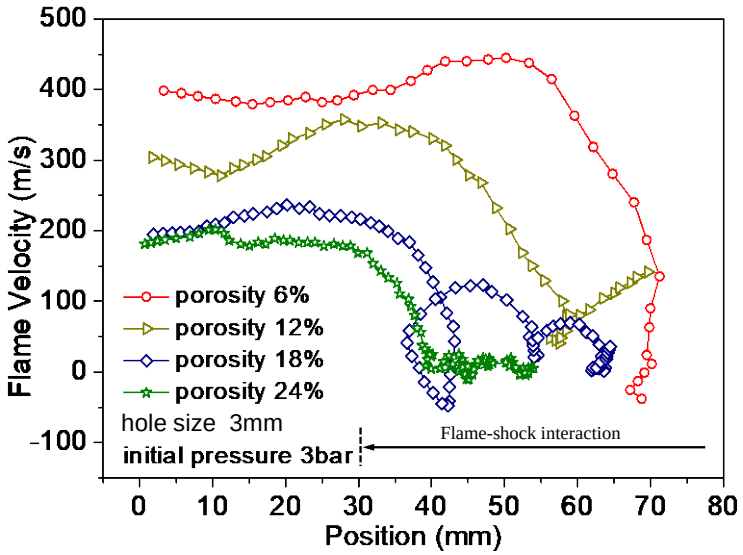

Fig. 11 Flame front velocity at different porosities, under conditions of hole size of 3 mm and initial pressure of 3 bar based on experimental setup A

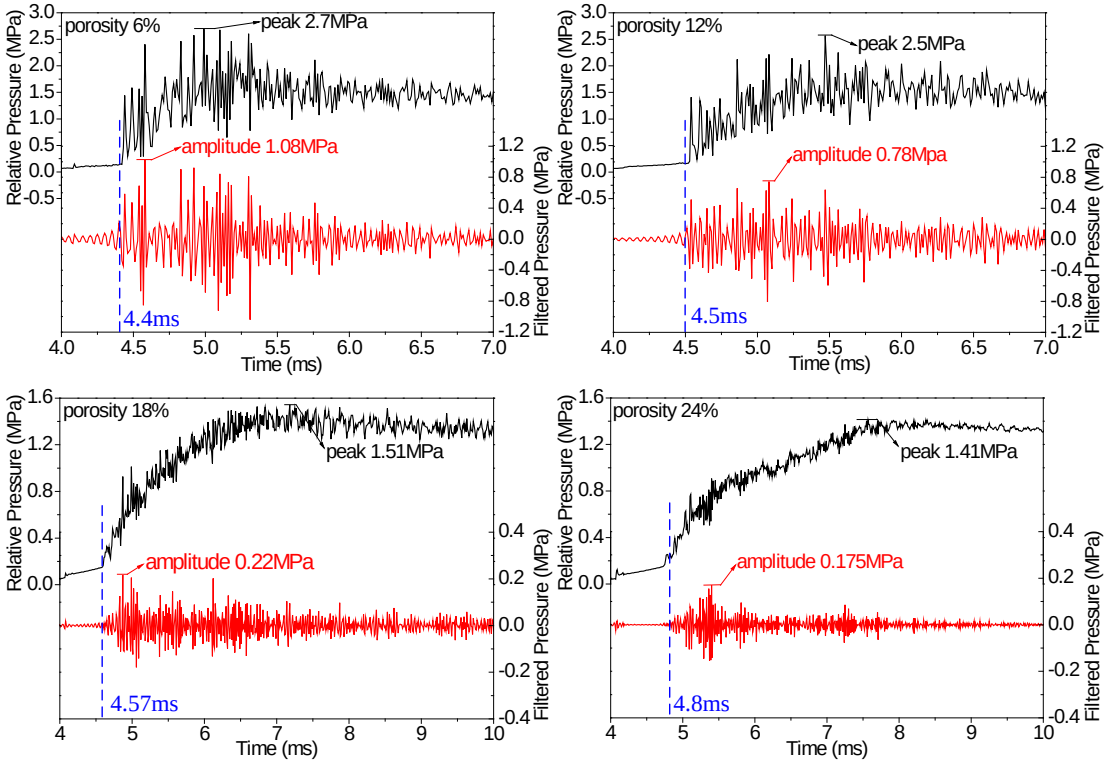

Fig. 12 Cylinder pressure at different porosities, under conditions of hole size of 3 mm and initial pressure of 3 bar based on experimental setup A

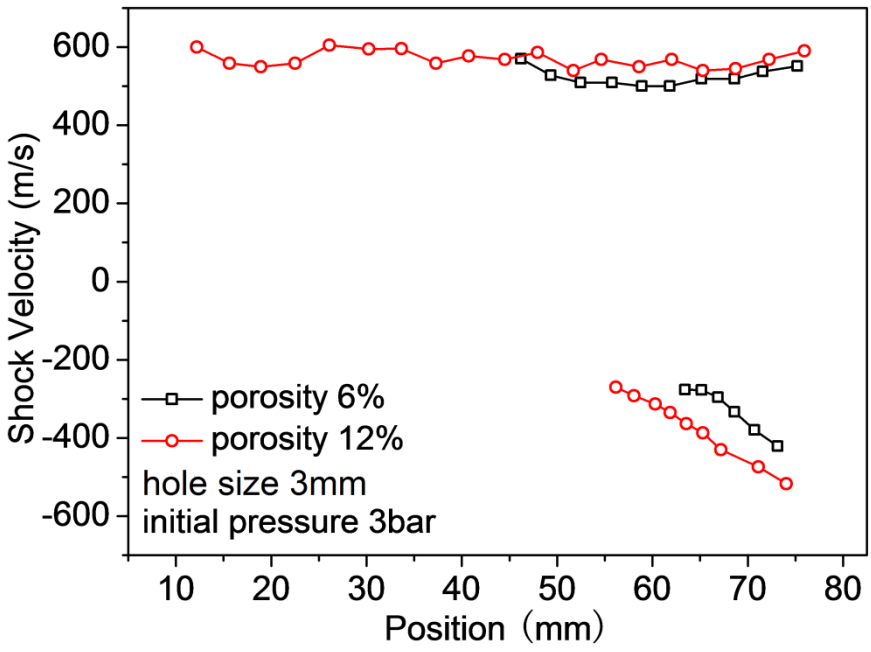

Fig. 13 Shock velocity at different porosities, under conditions of hole size of 3 mm and initial pressure of 3 bar based on experimental setup A

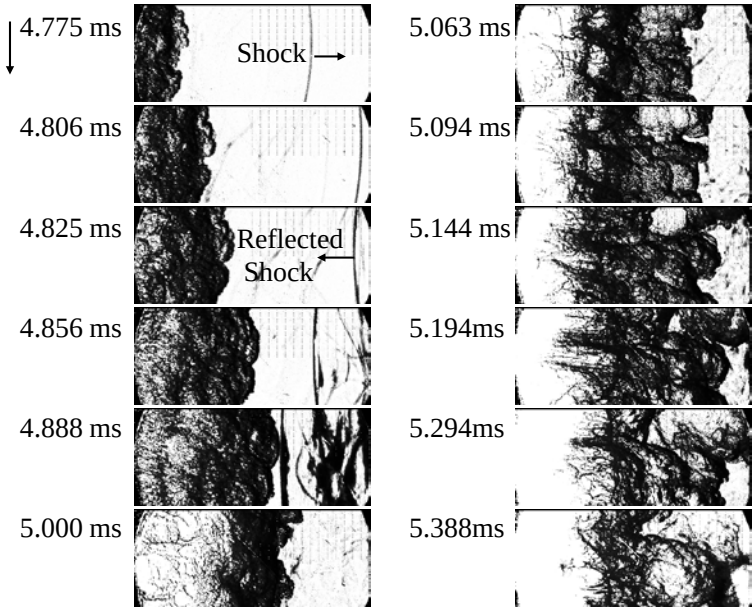

Fig. 14 Sequence of photography of flame and shock wave under conditions of hole size of 2.5 mm, porosity of 12%, and initial pressure of 3 bar based on experimental setup A

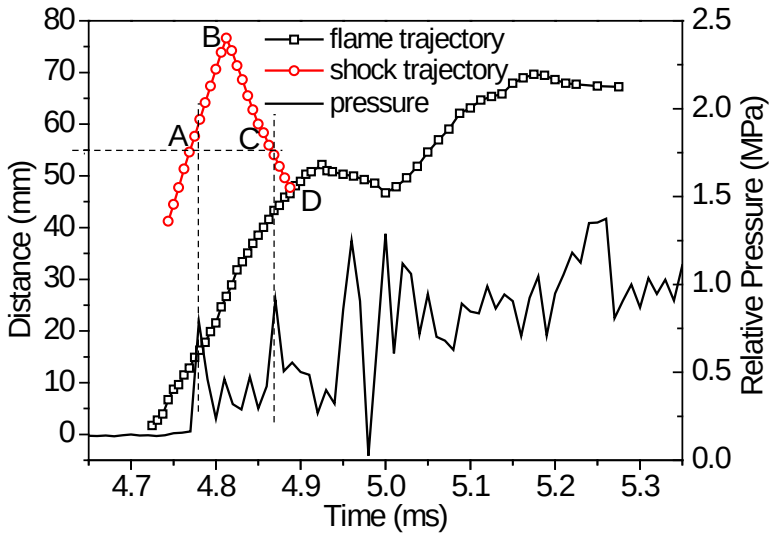

Fig. 15 Flame front trajectory, shock wave trajectory and pressure oscillation under conditions of hole size of 2.5 mm, porosity of 12%, and initial pressure of 3 bar based on experimental setup A. Note that point A and C represent the installation position of pressure transducer; point B represents the end wall of the chamber; point D represents the interaction of the reflected shock wave.

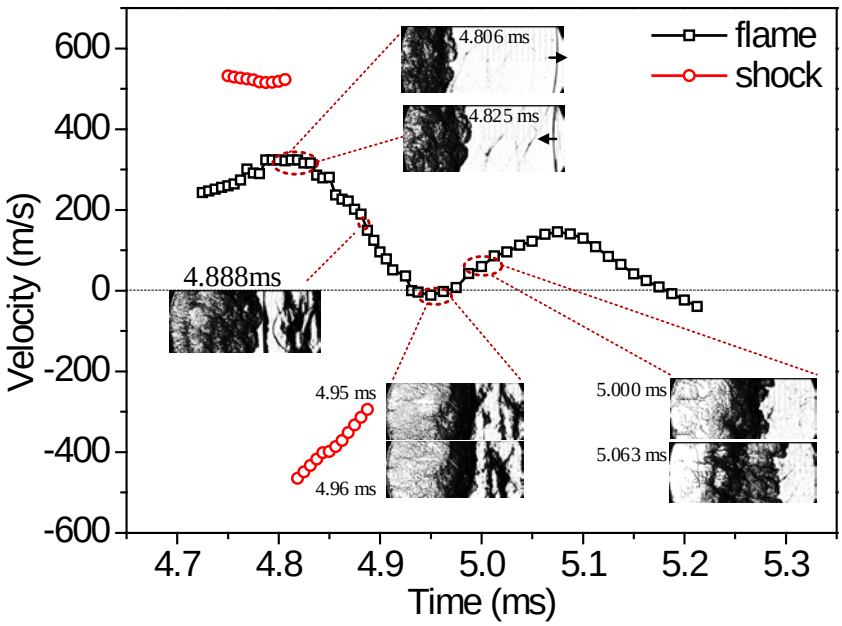

Fig. 16 Flame front velocity and shock wave velocity under conditions of hole size of 2.5 mm, porosity of 12%, and initial pressure of 3 bar based on experimental A

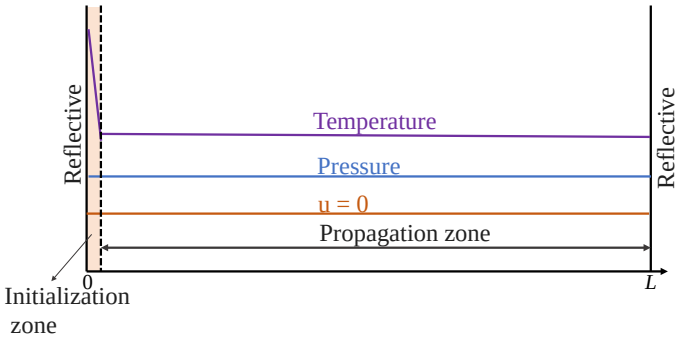

Fig.A1 The initial and boundary conditions in the case of flame-acoustic wave.

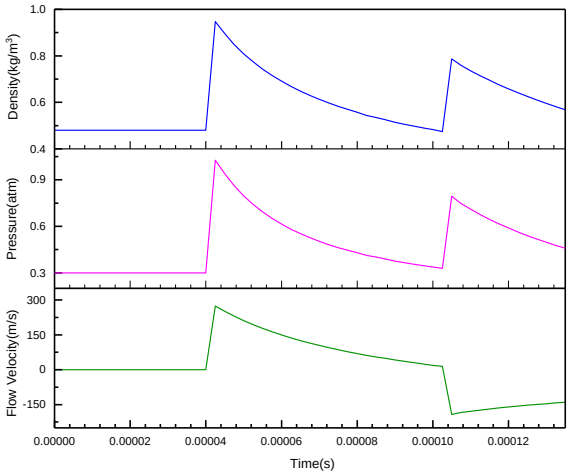

Fig.A2 Profiles of pressure, density and flow velocity versus time at the monitoring point in case 1

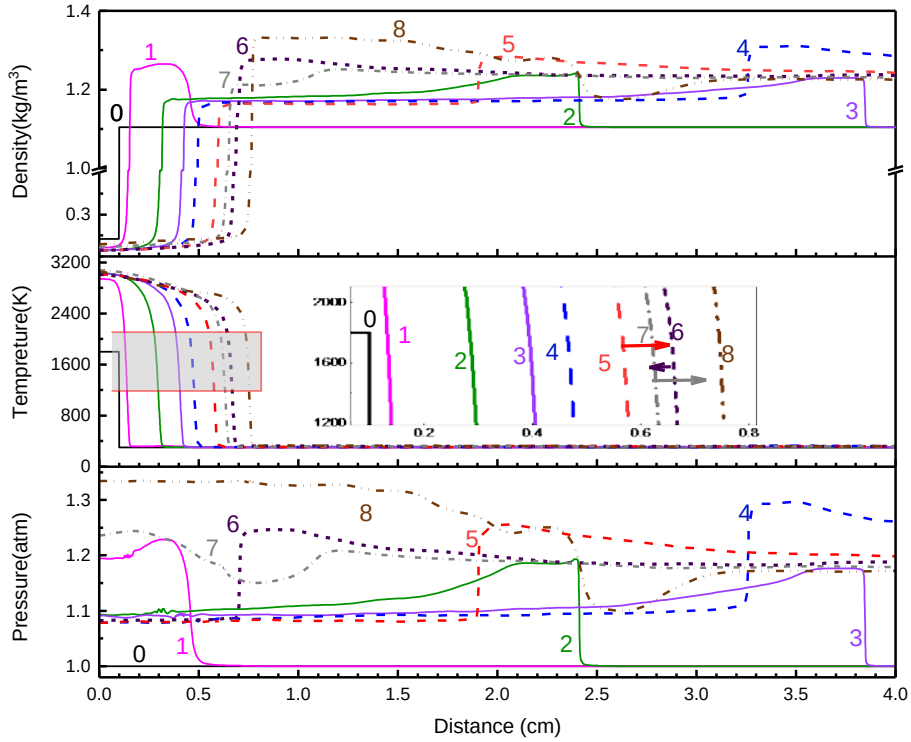

Fig.A3 Temporal evolution of density, temperature and pressure in the case 2. Line0 to line8 is: 0--0μs，1--8μs，2--64 μs，3--100μs，4--124μs，5-160μs，6-192μs，7-204μs，8-256μs

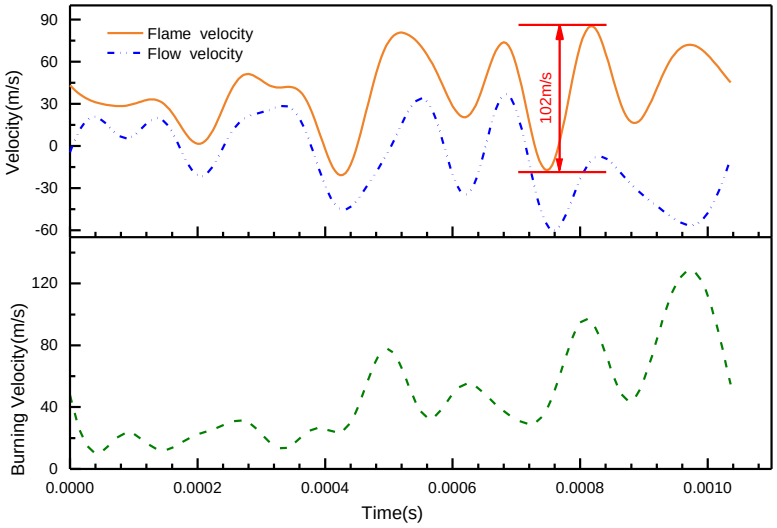

Fig.A4 Flame front velocity, flow velocity and burning velocity as a function of spatial position at 1 bar in the initialization zone in the case 2.

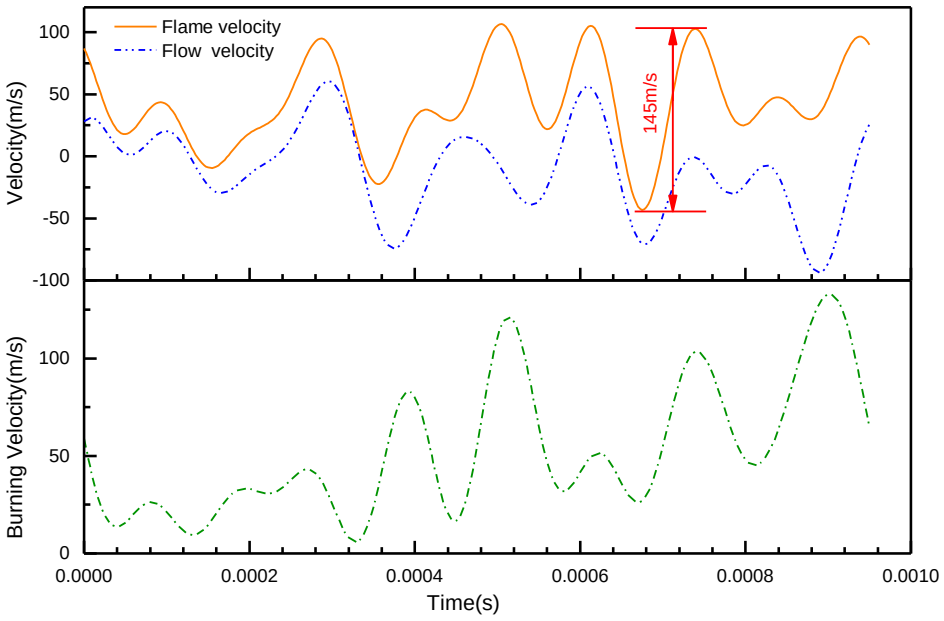

Fig. A5 Flame front velocity, flow velocity and burning velocity as a function of spatial position at 3 bar in the initialization zone in the case 2.

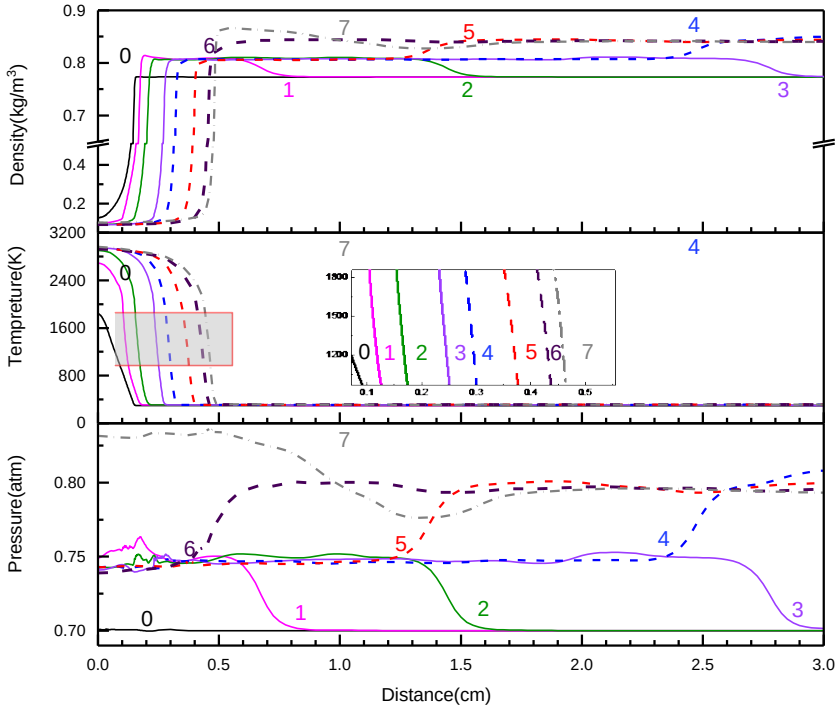

Fig.A6 Temporal evolution of density, temperature and pressure in the case 2. Line0 to line7 is: 0--0μs，1--25μs，2--45μs，3--80μs，4--100μs，5-130μs，6-155μs，7-185μs, repectively

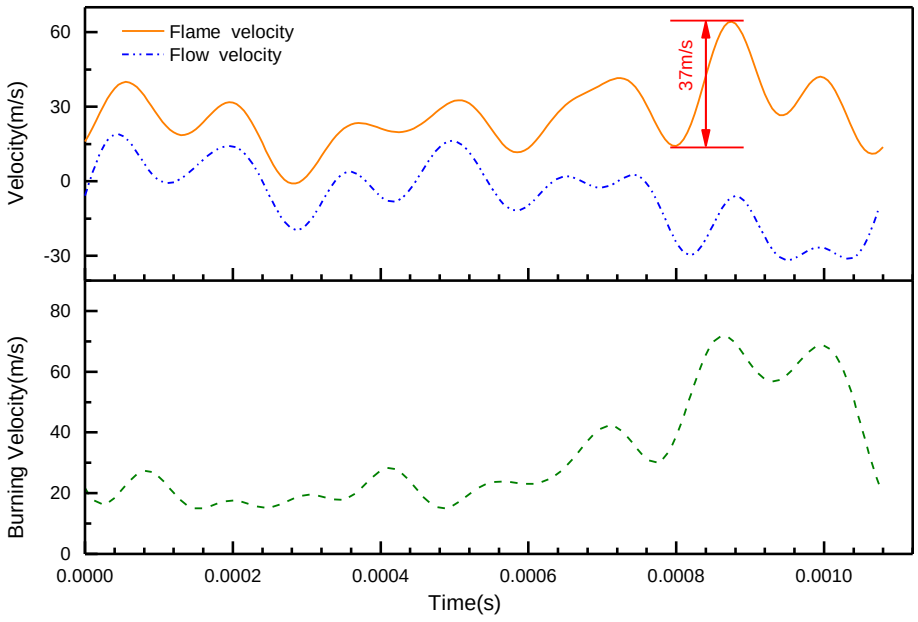

Fig. A7 Flame front velocity, flow velocity and burning velocity as a function of spatial position in the case 3.